Check for updates

A PVdF-based electrolyte membrane for a carbon counter electrode in dye-sensitized solar cells

Kyung Chul Sun, [ID] †[ab] Alvira Ayoub Arbab,†[cd] Iftikhar Ali Sahito, [ID] [cd]
Muhammad Bilal Qadir,[ce] Bum Jin Choi,[c] Soon Chul Kwon,[c] Sang Young Yeo,[b]
Sung Chul Yi*[af] and Sung Hoon Jeong [ID] *[c]

This research demonstrates the design and operation of a dye-sensitized solar cell (DSSC) with a multi-walled carbon nanotube counter electrode (CE) and a pore-filled membrane consisting of polyvinylidene fluoride-*co*-hexafluoropropylene (PVdF-*co*-HFP) as an electrolyte. In this cell, the internal resistance was substantially reduced and the efficiency was found to be as high as 6.04% under 1 sun. For this purpose, a sequence of experiments was carried out to demonstrate that the PVdF-*co*-HFP membrane possessed superior porosity to absorbed electrolytes and is more compatible with MWCNT CE as compared to the commonly used liquid electrolyte. For a comparison of results, different types of DSSC assemblies composed of MWCNT CEs were fabricated with liquid-, gel- and electrolyte-filled PVdF-*co*-HFP membranes. Morphological studies showed that the PVdF-*co*-HFP membrane is a regular and highly porous nano-web which provides optimized interfacial contact with defect-rich MWCNT CE. Detachment of the carbon particles from the CE causes short circuits and lower efficiency of the DSSCs. The proposed DSSC design not only lowers the interfacial charge transfer resistance ($R_{CT} = 2.98\ \Omega$) but also reduces the risk of short circuits in the cell. This sustainable and highly efficient DSSC structure provides a new method for the simple fabrication of flexible solar cells and electronic devices.

1. Introduction

The sustainable low-cost fabrication of dye-sensitized solar cells (DSSCs) has gained widespread attention owing to the invention of unique functional materials and facile fabrication techniques.[1–3] The standard DSSC assembly consists of meso-porous titania (TiO₂) as a photoanode with an adsorbed dye sensitizer, an iodide/triiodide redox liquid electrolyte mediator, and a platinum (Pt) counter electrode.[4–6] Typical DSSCs are associated with stability issues that result from their use of a platinum (Pt) cathode and liquid electrolyte, leading to poor stability, electrolyte leakage and electrode

corrosion. Moreover, the large-scale fabrication of DSSCs using Pt as a catalyst is hindered by the scarcity and high cost of Pt. Moreover, the Pt catalyst can disintegrate into PtI_4 in a liquid (I/I_3^-) electrolyte, which will reduce its long-term stability.[7,8] The interfacial charge transfer mechanism between a redox electrolyte mediator and a counter electrode plays an important role in DSSCs. Significant efforts have been undertaken to incorporate innovative, inexpensive, and rich materials with unique functional properties to fasten the interfacial charge transfer mechanism between the electrolyte and counter electrode using novel electrolytes and a low-cost electrocatalytic CE material.[9–12] Therefore, an ideal CE must have high electrocatalytic activity, good electrical conductivity, and a large surface area for rapid electrolyte/counter electrode interface reactions and long-term stability during chemical reactions.

Carbon-based electrocatalysts are gaining widespread attention due to their remarkable multifunctional properties.[13–16] Different carbon-based structures such as activated charcoal,[17–19] carbon black,[20,21] graphite,[22–24] graphene,[25–27] and carbon nanotubes[28–31] have been synthesized and have shown remarkable performance capabilities as counter electrode materials. MWCNTs are unique nanoscale structures with the distinct electronic features of high electrical conductivity and good chemical stability. MWCNTs can be considered as a fast electron-transport network owing to their coexistence tubular

ᵃDepartment of Fuel Cells and Hydrogen Technology, Hanyang University, Seoul 133-791, South Korea. E-mail: hytec@hanyang.ac.kr; scyi@hanyang.ac.kr

ᵇTechnical Textile & Materials R&D Group, Korea Institute of Industrial Technology, South Korea. E-mail: hytec@hanyang.ac.kr; miracle@kitech.re.kr

ᶜDepartment of Organic and Nano Engineering, Hanyang University, Seoul 133-791, South Korea. E-mail: alvira_arbab@yahoo.com; iftikhar.sahito@faculty.muet.edu. pk; ian8780@katri.re.kr; bilal_ntu81@hotmail.com; sckwon@kitech.re.kr; shjeong@ hanyang.ac.kr; Tel: +82222200498

ᵈDepartment of Textile Engineering, Mehran University of Engineering and Technology, Pakistan. E-mail: alvira_arbab@yahoo.com; iftikhar.sahito@faculty.muet.edu.pk

ᵉFaculty of Engineering & Technology, National Textile University, Faisalabad 37610, Pakistan. E-mail: bilal_ntu81@hotmail.com

ᶠDepartment of Chemical Engineering, Hanyang University, Seoul 133-791, South Korea. E-mail: scyi@hanyang.ac.kr

† These authors have equal contribution.

morphology and diffusive transport capabilities.[32,33] Moreover, MWCNTs possess high electrocatalytic activity for the reduction of triiodide ions to a certain extent, and their good mechanical properties can assist in the formation of matrix materials for constructing a fast electron-transport network.[34,35] Most commonly, oxidative functionalization or grinding by ball milling can be used to create a stable CNT dispersion. Unfortunately, these methods agglomerate CNT permanently due to their strong van der Waals forces and strong dispersants, which destroy the sp^2 structures.[36] To overcome this problem, we recently established an enzymatic route to synthesize a highly stable MWCNT dispersion without compromising on the electronic features.[37]

The adhesion of a MWCNT layer onto fluorinated tin oxide (FTO) glass is one of the key issues when it is used as a CE material. The conventional DSSC assembly consists of a liquid electrolyte mainly based on acetonitrile as a solvent, which can degrade the carbon layer, causing it to become detached from the FTO glass and thus leading to a short circuit in the cell. A schematic illustration of a short circuit in a cell using a carbon-based electrocatalyst is demonstrated in Fig. 1. For this purpose, a PVdF-*co*-HFP electro-spun nano-web was prepared and used as electrolyte-filled matrix in conjunction with the proposed MWCNT counter electrode.

In earlier work, the application of different membrane-based electrolytes in combination with a different counter electrode for DSSCs was proposed. These included a phthaloylchitosan-based gel polymer electrolyte,[38] a PVDF membrane-based electrolyte with an electrodeposited Pt counter electrode,[39] a PVDF–HFP electrolyte with different dyes,[40] and a PVDF–HFP gel electrolyte with a Pt counter electrode.[41] PVDF–HFP membrane electrolyte-based DSSCs have limited efficiency due to the lower ionic conductivity and low interfacial contact with the Pt CE. Herein, we propose the use of a carbon-based cathode with a defect-rich porous morphology in an effort to realize the fabrication of Pt-free and stable DSSCs. The suggested fabrication scheme of DSSCs provides ease of fabrication as well as a viable and stable design by providing an ionic conductive separator between the anode and the cathode to supersede the short-circuit frequency of the cells. Moreover, this scheme uses key materials and provides a fundamental study of the origins of electrical shorts. These results were also compared with those obtained with conventional liquid and polymer electrolytes in terms of the photovoltaic and electrochemical properties. The proposed DSSC system will provide new methods toward the fabrication of next-generation solar cells and flexible electronic devices.

2. Materials and methods

2.1 Materials

All chemicals used were of analytical grade. MWCNT powder with a carbon content exceeding 95%, 6–9 nm diameter, and 5 μm length (Sigma Aldrich Co.) was used. Lipase enzyme from candida rugosa, Type VII (Sigma Aldrich Co.), was used as an organic dispersant. Polymer carboxymethyl cellulose (sodium salt of M_W 250 000 g) was used as a binding agent. For the electrospinning of the PVdF-*co*-HFP electrolyte membrane, *N*,*N*-dimethylacetamide and acetone was purchased from Sigma Aldrich Co. Conductive transparent glass (FTO TEC 8, Pilkington Co.) substrates were used. Dye sensitizer D719, *cis*-di-isothiocyanato-bis (2,2′-bipyridyl-4,4′-dicarboxylato) ruthenium(II) bis(tetra butyl ammonium) from Everlight Chemical Co. was purchased. TiO$_2$ (P25 by Degussa Co.) 20 nm size was used for the photoanodes. Ionomer Surlyn with a thickness of 60 μm was purchased from Solaronix. Other reagents were purchased from Sigma Aldrich Co.
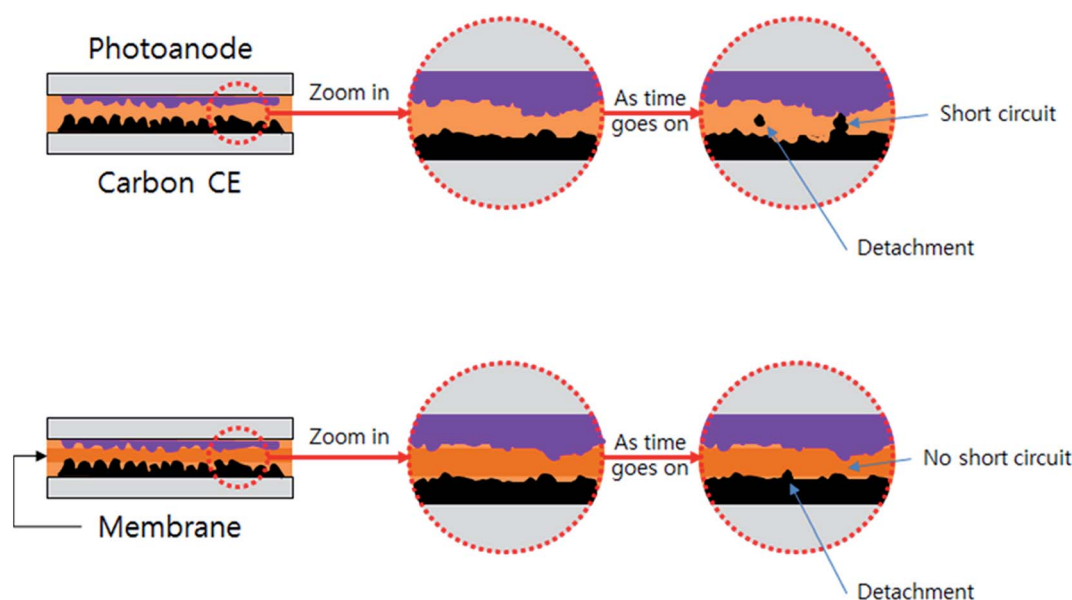

Fig. 1 Schematic illustration of a MWCNT-based CE and pore-filled membrane electrolyte demonstrating the possibility of no short circuits in cells.
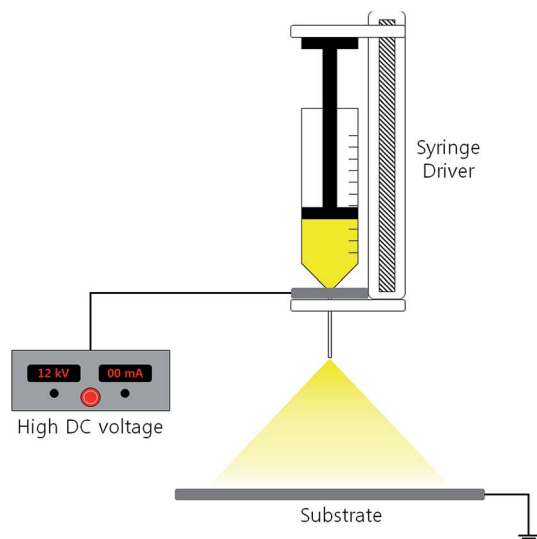
Fig. 2 Schematic illustration of the preparation for the electrospun PVDF-*co*-HFP membrane.

2.2 Fabrication of MWCNT counter electrodes

The carbon-based CE was prepared as follows. 0.4 g of MWCNT powder was dispersed in an ethanolic solution (1 mg mL^{-1}) containing lipase as an enzyme. The solution was stirred overnight and ultra-sonicated for two hours at room temperature. With ultra-sonication, the enzymes were physically adsorbed and entrapped onto the MWCNT surface, significantly releasing the MWCNTs with aggregation without disturbing their electronic characteristics. The carbon solution was then vacuum-filtered using a PTFE polymer membrane with a pore size of 0.5 μm followed by washing to remove enzyme byproducts. Afterwards, a 10 mL solution of a carboxy methyl cellulose solution was added to the carbon slurry and ground in an agate mortar to obtain a thick homogenous CNT paste. The MWCNT paste was then stored overnight at room temperature for aging. The FTO glass with sheet resistance of 8 Ω sq^{-1} was cleaned by sonication with acetone, distilled water, and ethanol for 15 min each. Carbon paste was coated onto the FTO glass under dry air at a temperature of 50 °C. A 3 μm layer thickness was maintained to avoid short circuits in the cell. The carbon electrodes were dried at 150 °C for 15 minutes and sintered at 300 °C for 30

minutes in a high-temperature furnace. Pt counter electrodes were prepared by drop-casting a 10 mM H$_2$PtCl$_6$ solution (in isopropanol) onto single-hole FTO glass with annealing at 400 °C for 20 minutes in a hot air blower.

2.3 Preparation of the pore-filled membrane electrolyte

The electrospun pore-filled PVDF-*co*-HFP membrane electrolyte was prepared as follows: a 15 wt% solution of PVDF-*co*-HFP was electrospun using *N,N*-dimethylacetamide and acetone at a ratio of 3 : 7. The solution was forced using a 25 G syringe pump and high voltage of 10 kV. The membrane was spun onto a stainless plate with a fixed distance of 20 cm from the end of needle. A 50 μm-thick membrane was prepared and used as an electrolyte medium. The resultant fibrous membrane was dried overnight in a vacuum chamber at 60 °C to remove any remaining solvent. Afterwards, the membrane was pressed to obtain a thick, even separator. The final thickness of the membrane was 30 μm. A schematic of the structure of the electrospinning system is shown in Fig. 2. For the liquid electrolyte, 1-butyl-3-methylimidazolium iodide (BMII), iodine (I$_2$), lithium iodine (LiI), and 4-*tert*-butylpyridine (TBP) were used. Polyethylene oxide (PEO) with a molecular weight of M_w 500 000 was added to form the gel electrolyte.

2.4 DSSC assembly

To fabricate the cell, the photoanodes were prepared according to the method used in our previous work.[42,43] The photoanodes and prepared CEs were fabricated by assembling a square cut piece of membrane. The DSSCs were sealed using an ionomer spacer with a hot presser at 80 °C for 20 seconds. After pressing, the electrolyte solution was injected from the holed CEs using a capillary vacuum effect. The cells were sealed with Surlyn and a cover glass. The resulting cells had an illuminated area of 0.2 cm^2 with black masking. A schematic diagram of the prepared DSSCs is shown in Fig. 3.

2.5 Characterization

The structural and morphological characteristics of the PVDF-*co*-HFP membrane and MWCNT samples were tested by a field emission-scanning electron microscope (FE-SEM, JEOL JSM-6700F) at an accelerating voltage of 15 kV. For the FE-SEM, all carbon samples were coated with Pt to improve the structural
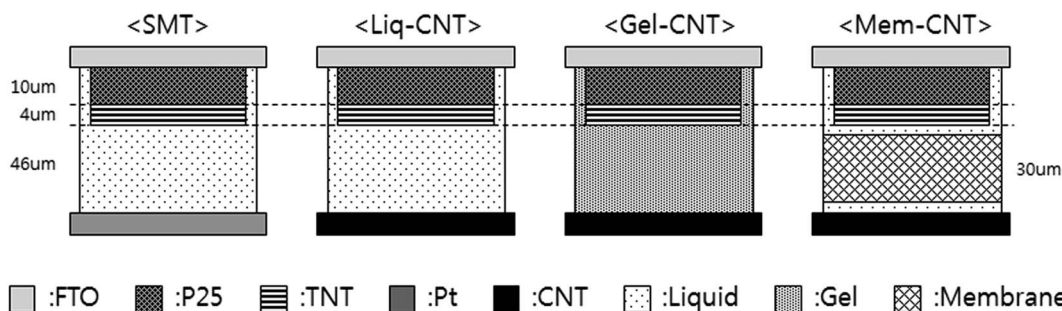

Fig. 3 Schematic illustration of DSSCs fabricated with Pt and MWCNT-based CE in combination of various types of electrolytes.

images. A standard four-point probe head system (RM3000 resistivity test unit by Jandel Engineering, Switzerland) was used to measure the electrical conductivity of the CEs. For an accurate examination of the thickness of the MWCNT layer on the FTO glass, an electronic outside micrometer (0–25 mm 0.01 mm) by Schut Geometrical Metrology was used. The cyclic voltammetry (CV) experiments were carried out using a three-electrode system in an argon-purged electrolyte (0.01 M $LiClO_4$, 10 mM LiI, and 1 mM I_2 prepared in an acetonitrile solution) at a scan rate of 20 mV s^{-1} with an Ultimate Electrochemical Workstation (Bio Logic Science Instruments). A diffusion constant of I_3^- was determined by cyclic voltammogramety at a scan rate of 5 mV s^{-1}. The ionic conductivity of the electrolyte and the charge transfer resistance properties of the CEs were measured by the symmetrical cell technique with electrochemical impedance spectroscopy. The photovoltaic performance capabilities of DSSCs fabricated with different CEs were evaluated using a K101-Lab 20 source measuring unit (Mac Science Co.). A solar simulator with a 160 W Xenon arc lamp was used as a light source (spectral match; 0.75–1.25, non-uniformity of irradiance; ≤±2 percentage, temporal instability; ≤±2%). The light intensity was calibrated with a KIER-calibrated Si solar cell (Mac Science Co.). The photovoltaic parameters of the cells were measured under a masked frame.

3. Results and discussion

The scanning electron microscope (SEM) image shown in Fig. 4 depicts the three-dimensional network of the tubular MWCNT matrix. The nano-patterned carbon structure revealed at low magnification shows the highly convoluted matrix of CNTs. The high-magnification image shows an interconnected MWCNT
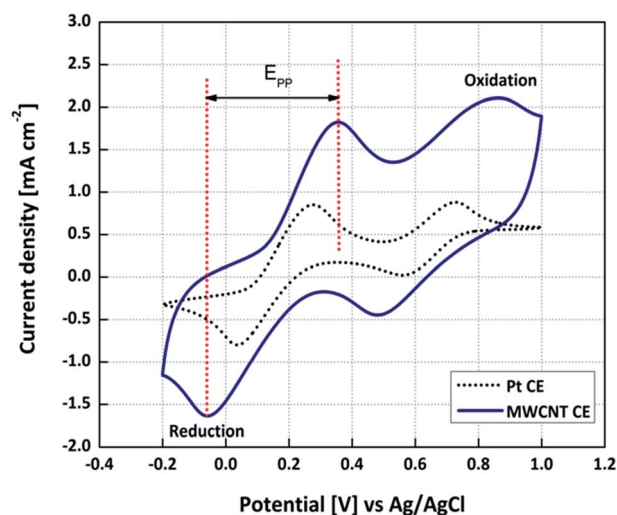
Fig. 6 Cyclic voltammograms of the Pt and MWCNT counter electrode.

network structure, which provides faster electrical charge transport. This MWCNT structure is essential for good electrical conductivity and a high surface area. The cross-sectional FE-SEM image shows a high density defect-rich edge surface, which is responsible for the improved electrode-membrane electrolyte interface and lower charge transfer resistance (R_{CT}) of the carbon CEs.[44] The MWCNT demonstrated low adhesion and detachment with the liquid electrolyte in a suitable amount of time. Hence, it is necessary to find alternative methods by which to realize sustainable DSSC structures for high efficiency and sustainability.
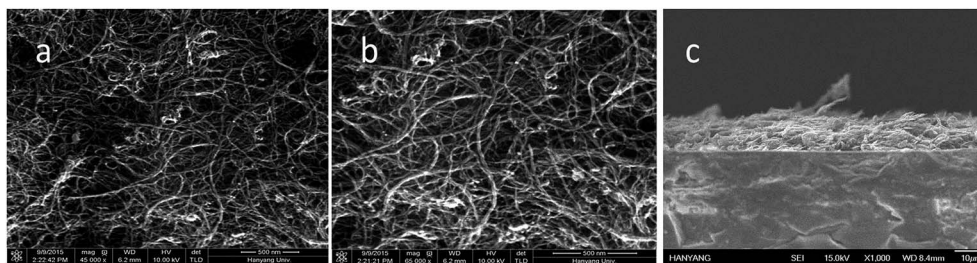
Fig. 4 (a) Surface morphology of the MWCNT layer, (b) high-magnification image, and (c) cross-sectional image of the MWCNT electrode.
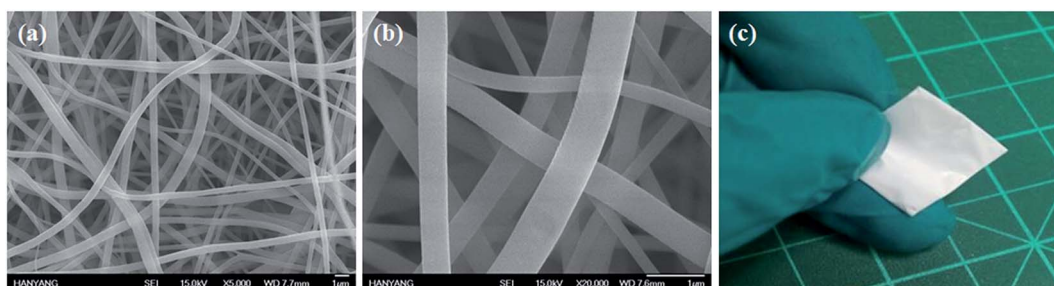
Fig. 5 FE-SEM image of the electrospun PVdF-co-HFP membrane used as the pore-filled electrolyte.
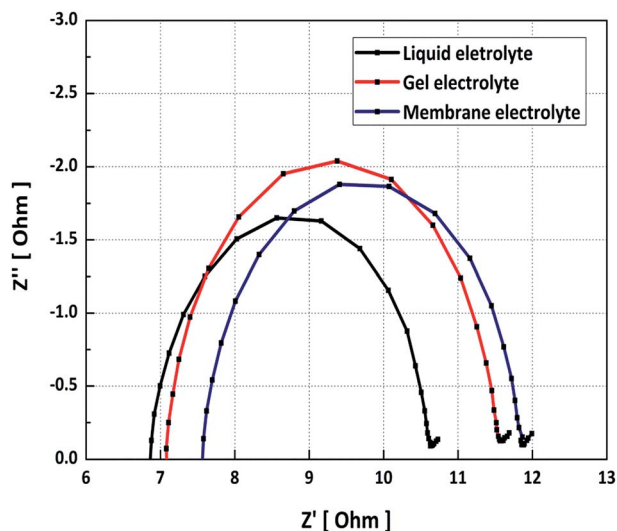
Fig. 7 Electrolyte bulk resistances in the frequency range of 0.1 Hz to 100 kHz with AC oscillation of 10 mV.
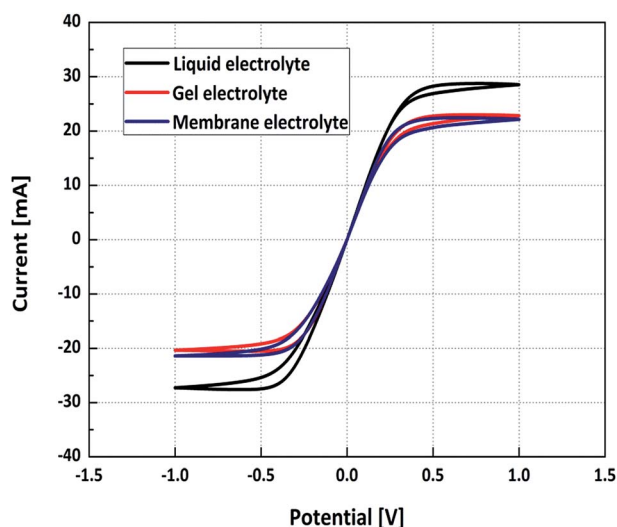

Fig. 8 Steady-state current–potential curve of the symmetrical cells using different electrolyte types.

Fig. 5 shows a FE-SEM image of the prepared electrospun membrane used as the pore-filled electrolyte matrix. It consists of a nano-fibrous web with an average diameter of 500 nm. The PVdF-*co*-HFP membrane shows a porous dimensional interconnected network. This membrane has high porosity and

a fully interconnected 3D network structure. The proposed membrane has a pore area of 25.610 m^2 g^{-1} with an average pore diameter of 0.607 μm. The apparent density was 1.2806 g mL^{-1} and the porosity was 84.0081%. These characteristics of the PVdF-*co*-HFP membrane will provide sufficient electrolyte wicking inside its porous structure.

The electrical resistivity levels of the MWCNT and the Pt electrode were also measured. The sheet resistance of the carbon electrodes was 6 ± 0.5 Ω sq^{-1}, which was even lower than that of Pt at 7 Ω sq^{-1}. Such lower resistance indicates that this electrode can be potentially applied to CE, which would be very useful as it could then replace the expensive Pt electrode.

The major role of CE in a DSSC is as a catalyst that effectively regenerates reduced species in the electrolyte, but at the same time it also provides a pathway for the photocurrent to complete the circuit. Therefore, both the catalytic properties of the CE towards the redox couple and the conductivity of the CE substrate are essential for good CE performance. We initially conducted cyclic voltammetry (CV) measurements in a three-electrode system to investigate the catalytic properties. The synergic nature of the MWCNT CE with high conductivity and a defect-rich structure is expected to lead to improved electro-catalytic activity (ECA) towards the reduction of the I$_3^-$ species to I$^-$ at the counter electrode.[45] Cyclic voltammetry (CV) tests were carried out to evaluate the electrocatalytic properties of the MWCNT CE. To identify the electrocatalytic activity of the CE, cyclic voltammetry (CV) was utilized in a three-electrode system in 0.01 M LiClO$_4$, 10 mM LiI, and 1 mM I$_2$ in an acetonitrile solution.[46] The CV curves of different CEs using the three-electrode method are presented in Fig. 6. Two distinctive sets of oxidation and reduction peaks were observed for the Pt and MWCNT CEs, respectively. A negative (cathodic) peak was assigned to the reduction reaction (eqn (1)) and a positive anodic peak was assigned to the oxidation reaction[47] (eqn (2)).
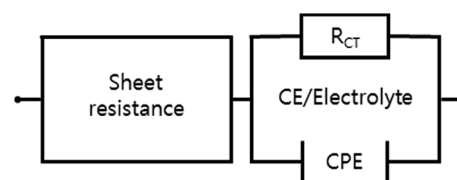
$$I_3^- + 2e^- \rightarrow 3I^- \tag{1}$$

Fig. 10 Equivalent circuits for the EIS measurement of the symmetrical cells.
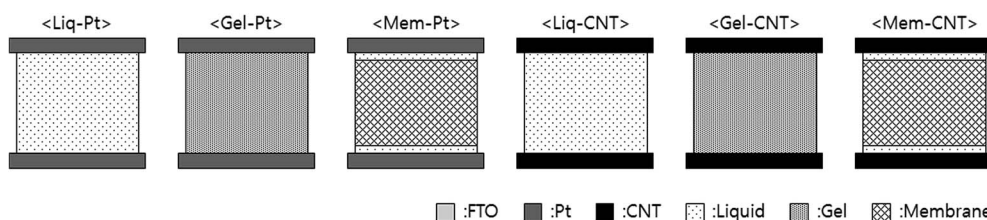
Fig. 9 Schematic illustrations of symmetrical cells.

$$3I_2 + 2e^- \rightarrow 2I_3^- \tag{2}$$

The ECA of an electrocatalyst toward reduction can be visualized in terms of its cathodic peak potential (E_{cp}) and cathodic peak current density (I_{pc}) in a CV diagram. MWCNT reveals higher I_{pc} values with more positive E_{cp} values and possesses the higher electrocatalytic activity than Pt CE. Moreover, the peak-to-peak separation (E_{pp}), which is inversely proportional to the standard electrochemical rate constant of the I$^-$/I$_3^-$ redox reaction, is an important factor when investigating the ECA of the CE.[48] MWCNT CE has a smaller E_{pp} (0.30 V) value, equal to that of a conventional platinized FTO CE (0.24 V), indicating the intrinsic electrocatalytic activity of MWCNT towards the iodide/triiodide redox reaction. The porous morphology and high oxygen level over the MWCNT surface due to enzyme overlapping tend to amplify the absorption of iodide ions over the carbon layer with reduction back onto the surface. The oxygen-rich porous surface of the MWCNTs has higher triiodide reduction than the reference Pt catalyst. This investigation finds that a higher electrocatalytic surface area can be achieved in the proposed carbon-based CE.

The ionic conductivity of the electrolyte, σ, was calculated by the following equation,

$$\sigma = \frac{l}{RA} \ [\text{S cm}^{-1}], \tag{3}$$

where l is the thickness of the web, R is the bulk resistance of the electrolyte, and A is the area of the web. The bulk resistance was calculated from the EIS spectra of identical symmetrical cells. The diameter of the semicircles determined the bulk resistance of the electrolyte, as shown in Fig. 7. The ionic conductivity of the membrane electrolyte was measured and found to be 2.31×10^{-3} S cm^{-1} at room temperature, which is quite close to that of the liquid electrolyte at 2.67×10^{-3} S cm^{-1}. 5 wt% of a PEO-based gel electrolyte showed a value of 2.21×10^{-3} S cm^{-1}. The polymeric content in the electrolyte tends to decrease the ion mobility and affect the ionic conductivity. Therefore, gel-based electrolytes have less ionic conductivity as compared to liquid- and membrane-based electrolytes. The ionic conductivity of the membrane-based electrolyte was slightly greater as compared to the gel-type electrolyte. The PVDF–HFP membrane was soaked with the liquid electrolyte and used in the DSSCs. Hence, the membrane showed higher ionic conductivity and greater ionic mobility when the membrane was soaked in this electrolyte medium.

The diffusion constant of the electrolyte is also valuable when used to define the interference between the electrolyte and the CE surface. The diffusion constants of I$_3^-$ were measured using symmetrical CEs cells with cyclic voltammograms at a scan rate of 5 mV s^{-1}. These results are shown in Fig. 8. The diffusion-limited current is proportional to the diffusion constants of I$_3^-$, denoted by $D_{I_3^-}$ and obtained through the following equation:

$$D_{I_3^-} = \frac{I_{lim} \times l}{2 \times n \times F \times C_{I_3^-} \times A} \ [\text{cm}^2 \ \text{S}^{-1}] \tag{4}$$
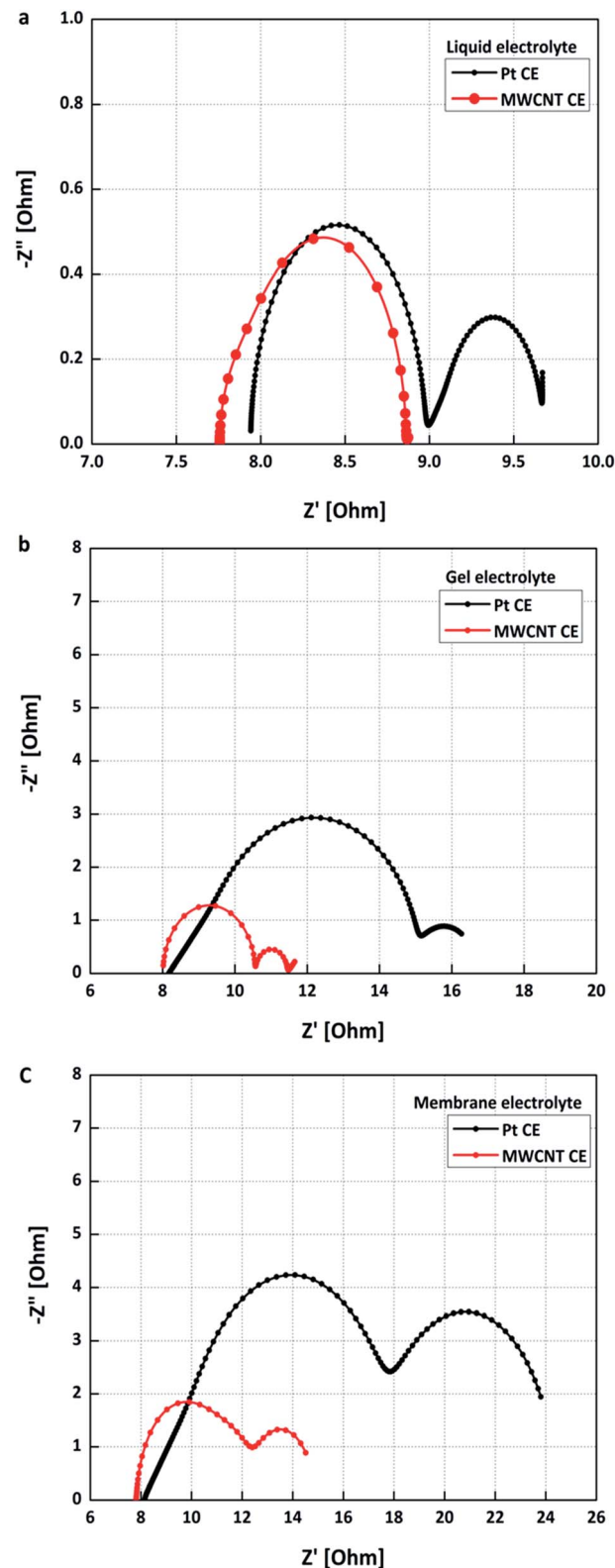

Fig. 11 Nyquist plot obtained for symmetrical cells of Pt- and MWCNT-based CEs fabricated with (a) a liquid, (b) a gel polymer and (c) a fibrous membrane electrolyte.

Table 1 Electrochemical and photovoltaic performance capabilities of cells fabricated with MWCNT counter electrodes in combination with different electrolytes types

| Electrolyte/MWCNT	Symmetrical cells			DSSC		
	R_{S} (Ω)	R_{CT} (Ω)	V_{OC} (V)	J_{SC} (mA cm^{-2})	FF (%)	PCE (%)
Liquid	7.74	0.50	0.714	12.591	74.17	6.66
Gel	7.99	0.87	0.747	11.215	68.88	5.77
Membrane	7.78	2.98	0.716	12.097	69.81	6.04

Table 2 Electrochemical and photovoltaic performance capabilities of cells fabricated with Pt counter electrodes in combination with different electrolyte types

Electrolyte/Pt	Symmetrical cells			DSSC		
	R_{S} (Ω)	R_{CT} (Ω)	V_{OC} (V)	J_{SC} (mA cm^{-2})	FF (%)	PCE (%)
Liquid	7.93	0.64	0.684	14.075	76.09	7.32
Gel	8.13	6.00	0.703	13.156	73.89	6.83
Membrane	8.18	6.60	0.670	13.143	74.28	6.53

here, I_{lim} denotes the diffusion-limited current, n is the number of electrons transferred, F is the Faraday constant, and $C_{I_3^-}$ is the concentration of I_3^-. The diffusion constant of the liquid electrolyte was 1.48×10^{-5} cm^2 S^{-1}. However, the gel and membrane electrolytes showed diffusion constants of 1.18×10^{-5} cm^2 S^{-1} and 9.71×10^{-6} cm^2 S^{-1}, respectively. The ionic conductivity of the electrolyte is related to the internal transport kinetics between CE and the I_3^-/I^- ratio of the electrolyte and the photocurrent density of the DSSCs.[49]

Another method which can be used to probe the electrochemical performance of CE is to employ a symmetrical cell configuration (*i.e.*, a sandwich structure of CE/electrolyte/CE) which resembles the typical DSSC device structure but without the anode electrodes so as to avoid the impedance loss of the dye-loaded TiO$_2$ working electrode. This structure provides a practical environment for testing the CE.[50] In order to determine the interfacial charge transfer resistance (R_{CT}) between CE and different types of electrolytes, three different symmetrical dummy cells composed of liquid-, gel- and fibrous-membrane-based electrolytes were prepared. Schematic illustrations of the symmetrical cells are shown in Fig. 9. A Randles-type equivalent circuit was used to fit the semicircles obtained in the EIS shown in Fig. 10. Two semicircles were observed in the spectra; the semicircle observed in the low-frequency region (right) is the Nernst diffusion impedance in the electrolyte and the semicircle in the high-frequency region (left) is the interfacial charge transfer resistance (R_{CT}) of CE.

Nyquist plots of the respective CEs are shown in Fig. 11. The results obtained for the MWCNT and Pt electrodes are tabulated Tables 1 and 2, respectively. The R_{CT} values of the cells with the electrolytes based on liquid, gel and the membrane, with MWCNT as the CE, were found to be 0.50 Ω, 0.87 Ω and 2.98 Ω, respectively. Thus, there is a major reduction in the charge-transfer resistance when using the MWCNT (2.98 Ω) instead of Pt (6.60 Ω) as a catalytic layer, producing a significant benefit for the performance of the membrane-based DSSCs. More specifically, in addition to the fill factor, the V_{OC} appears to
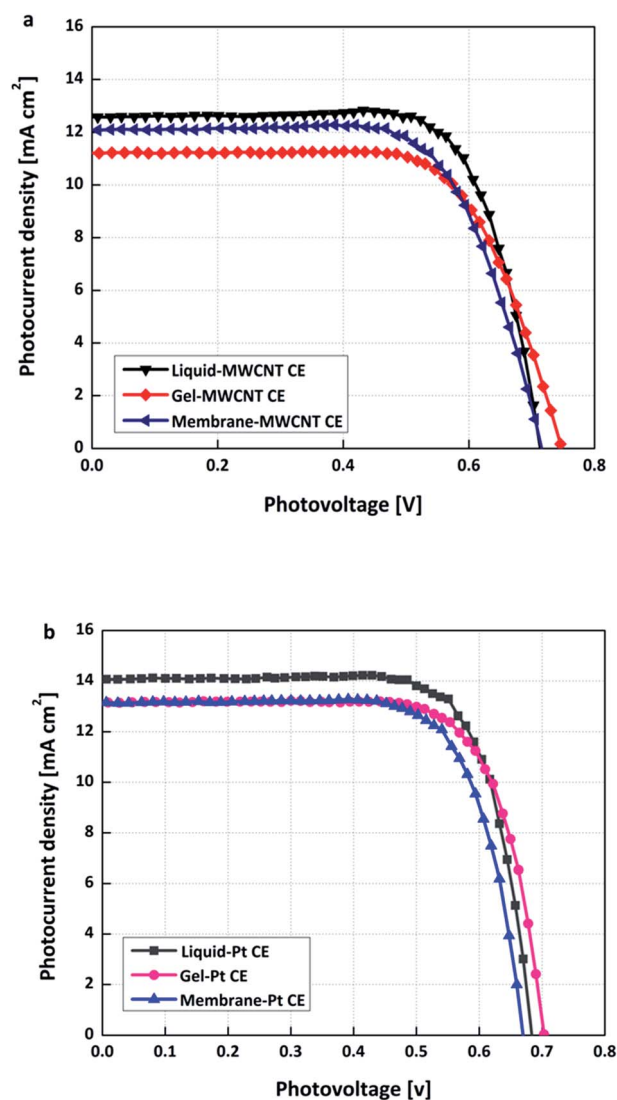
Fig. 12 Polarization curve of DSSCs fabricated with different electrolyte types in a combination of (a) MWCNT- and (b) Pt-based CEs under 1 sun illumination.

improve with a decrease in R_{CT}. As identical MWCNT electrodes were used for each cell, different interfacial reactions of the electrolyte and counter electrode are responsible for the different R_{CT} values. These results demonstrated that carbon-based CE possesses a highly dispersed and well-ordered conductive network of MWCNTs which can reduce the R_{CT} of CE in symmetrical cells. The defect-rich porous morphology of the MWCNT CE provides better accessibility towards iodide ions. Therefore, volatile liquid-based electrolytes can be replaced with a pore-filled PVdF-*co*-HFP membrane electrolyte when the cells are fabricated with carbon-based CE.

The photovoltaic performances of the membrane-based DSSCs were investigated by fabricating cells with and without MWCNT CEs, with a subsequent comparison with Pt cells. The photocurrent–voltage (*I–V*) curves of different CEs were measured under simulated AM 1.5 illumination (1 sun, 100 mW cm^{-2}). The photocurrent density (J_{SC}), open-circuit voltage (V_{OC}), fill factor (FF) and power conversion efficiency (η) of the cells are listed in Tables 1 and 2. Eight cells in total were fabricated. Optimized values are tabulated in Tables 1 and 2.

The power conversion efficiency (PCE) of DSSCs can be calculated using the following equation.

$$PCE = V_{OC} \times J_{SC} \times FF \qquad (5)$$

The DSSCs fabricated with the MWCNT CE and showed better performance with the membrane electrolyte and are comparable to Pt electrodes. It was found that DSSCs based on MWCNT CEs fabricated with the membrane electrolyte showed higher V_{OC} (0.716 V), J_{SC} (12.097 mA cm^{-2}) and FF (69.81%)

values, with an efficiency rate of 6.04%. This performance of the device is likely due to the low charge transfer resistance (2.93 Ω) and higher electrocatalytic activity at the CE with the membrane electrolyte, as confirmed by the EIS and CV analyses. In brief, the MWCNT-based DSSCs exhibit better performance and can replace the assembly of Pt and liquid electrolyte in the cells. Higher V_{OC} values were observed for the MWCNT-based DSSCs. According to results presented in Table 1, the DSSC based on MWCNT CE fabricated with the gel type electrolyte showed a high V_{OC}. The gel type will sustain the stable porous morphology of the carbon CE, while the liquid electrolyte is rapidly absorbed due to the high surface area. Membrane electrolytes have limited ionic conductivity and less dissipation of iodide species on C surfaces. Therefore, gel-type electrolytes have high V_{OC} values when fabricated with MWCNT CEs. The morphological structure of carbon-based CEs provides more accessibility for triiodide ions to penetrate into the structure and become reduced onto the CE surface. However, slightly lower values of FF arise due to the bulk membrane used during the cell fabrication process. DSSCs fabricated with liquid show efficiency rates of 6.66%. However, low performance was noted with gel-based electrolytes, which showed an efficiency rate of 5.77%. Low electrolyte penetration into the conductive layer of the CE reduced the FF and J_{SC} values. The *I–V* curve of MWCNT-based DSSCs is shown in Fig. 12a. The results are tabulated in Table 1.

It was observed in the results that the Pt CEs possess low surface areas and low electrocatalytic activity, which cause a reduction of I_3^- species at the CE and subsequently lower the V_{OC} value of membrane-based cells. Fig. 12b presents the *I–V*
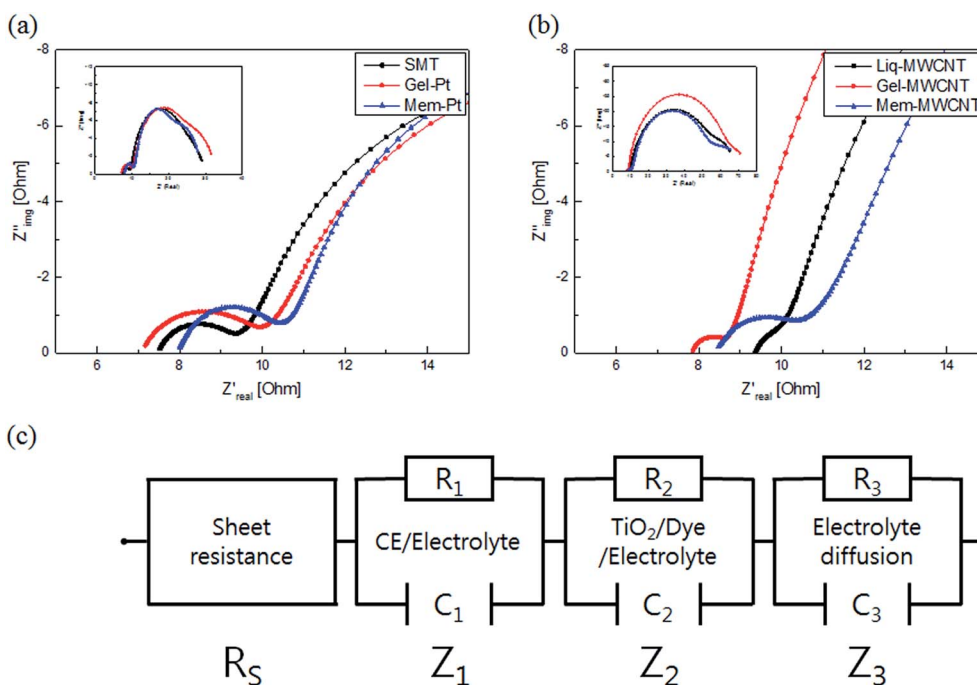

Fig. 13 Nyquist plot of the electrochemical impedance spectroscopy in DSSCs fabricated with different types of electrolytes in combinations of (a) Pt- and (b) MWCNT-based CEs under 1 sun illumination. (c) Equivalent circuit of the cell, consisting of a metal substrate (FTO), a counter electrode/redox electrolyte interface, a photoanode/redox electrolyte interface and electrolyte diffusion.

curves of DSSCs based on Pt CE fabricated with different types of electrolytes. The results are tabulated in Table 2. The cell fabricated with the conventional Pt CEs showed efficiency of 7.32%, whereas the efficiency for the cell prepared with the gel electrolyte was 6.83%. In contrast, the membrane-based DSSCs demonstrated 6.53% efficiency, which is close to the suggested low-cost DSSCs system. Specifically, the open-circuit voltage (V_{OC}) values were lower with the Pt CEs. The Pt-CE-based cells fabricated with the gel-type electrolyte showed the highest V_{OC} values (Table 2). The liquid electrolyte rapidly evaporates from the cells; however, the PEO-based gel electrolyte has good sustainability. Hence, Pt CE fabricated with a gel-type electrolyte has higher V_{OC} values.

These results indicate the fast electron mobility at the FTO/MWCNT/membrane electrolyte interface, resulting in high photovoltage (V_{OC}), and FF values. Comparing the results of the photocurrent and diffusion coefficient of I_3^-, an increase in J_{SC} with different types of electrolytes was found to be related to the improved diffusion of I_3^-.

The prepared DSSCs are analyzed by electrochemical impedance spectroscopy (Fig. 13) with an equivalent circuit model (Fig. 13c). In the results, the first circle can provide useful information about the inter kinetics between the counter electrode and the electrolyte. In the platinum graph, they show the impedance value (in the first circle) according to the sequence of liquid < gel = membrane electrolyte. This indicates that the interfacial resistance levels of the gel/Pt and membrane/Pt samples are higher than that of the liquid/Pt sample. In the MWCNT graph, they show a corresponding order of liquid/MWCNT = gel/MWCNT < membrane/MWCNT, indicating that the interfacial resistance of the membrane/MWCNT sample is higher than those of the other cases. Therefore, it can be said that the connection between the membrane and the MWCNTs can create higher impedance as compared to a gel or liquid electrolyte, which may explain the increased first circle size in the EIS. Specifically, the first circles of the MWCNT-based cells are smaller than those of the platinum-based cells.

4. Conclusion and future suggestions

An electrospun PVdF-*co*-HFP membrane was prepared and used as a pore-filled electrolyte matrix for MWCNT CEs. The unique nanostructure of the MWCNT CEs, including a large surface area and a network structure along with a high interconnected interracial reaction mechanism, guaranteed rapid mass transport for electrolyte and enabled the CE to accelerate the reduction of triiodides to the iodide present in the porous PVDF-*co*-HFP membrane. The extensive electrochemical analyses of MWCNT CE with the membrane electrolyte *via* CV and EIS measurements also indicated lower charge transfer resistance of 2.98 Ω at the CEs. The proposed design of DSSCs assembled with MWCNT CEs and a pore-filled membrane electrolyte exhibited a power conversion efficiency of 6.04% under AM 1.5 illumination at 100 mW cm^{-2}, comparable to that of DSSCs based on the conventional design with a liquid electrolyte with Pt CEs (7.32%). If it is possible to prepare a thinner and stronger membrane, useful information can be gleaned

from the findings here. As a suggestion for future work, this cell design can be realized by the direct deposition of an electrospun membrane on the counter electrode, which may be scalable as a one-step continuous process. The proposed DSSC design suggests that MWCNT-based CEs and membrane-electrolyte-based cells shows great potential for use in low-cost and flexible electronic devices.

Acknowledgements

References

1 H. Yu, B. Xue, P. Liu, J. Qiu, W. Wen, S. Zhang and H. Zhao, High-Performance Nanoporous TiO_2/La_2O_3 Hybrid Photoanode for Dye-Sensitized Solar Cells, *ACS Appl. Mater. Interfaces*, 2012, **4**, 1289–1294.

2 N. Sakai, T. Miyasaka and T. N. Murakami, Efficiency Enhancement of ZnO-Based Dye-Sensitized Solar Cells by Low-Temperature $TiCl_4$ Treatment and Dye Optimization, *J. Phys. Chem. C*, 2013, **117**, 10949–10956.

3 M. Grätzel, Solar Energy Conversion by Dye-Sensitized Photovoltaic Cells, *Inorg. Chem.*, 2005, **44**, 6841–6851.

4 S.-H. Liu, H. Fu, Y.-M. Cheng, K.-L. Wu, S.-T. Ho, Y. Chi and P.-T. Chou, Theoretical Study of N749 Dyes Anchoring on the $(TiO_2)_{28}$ Surface in DSSCs and Their Electronic Absorption Properties, *J. Phys. Chem. C*, 2012, **116**, 16338–16345.

5 G. Yue, J. Wu, Y. Xiao, J. Lin, M. Huang and Z. Lan, Application of Poly(3,4-Ethylenedioxythiophene):Polystyrene sulfonate/Polypyrrole Counter Electrode for Dye-Sensitized Solar Cells, *J. Phys. Chem. C*, 2012, **116**, 18057–18063.

6 U. Mehmood, I. A. Hussein, K. Harrabi, M. B. Mekki, S. Ahmed and N. Tabet, Hybrid TiO_2–Multiwall Carbon Nanotube (MWCNTs) Photoanodes for Efficient Dye-Sensitized Solar Cells (DSSCs), *Sol. Energy Mater. Sol. Cells*, 2015, **140**, 174–179.

7 Y. Xie, P. Joshi, S. B. Darling, Q. Chen, T. Zhang, D. Galipeau and Q. Qiao, Electrolyte Effects on Electron Transport and Recombination at ZnO Nanorods for Dye-Sensitized Solar Cells, *J. Phys. Chem. C*, 2010, **114**, 17880–17888.

8 A. A. Arbab, K. C. Sun, I. A. Sahito, M. B. Qadir, Y. S. Choi and S. H. Jeong, A Novel Activated-Charcoal-Doped Multiwalled Carbon Nanotube Hybrid for Quasi-Solid-State Dye-Sensitized Solar Cell Outperforming Pt Electrode, *ACS Appl. Mater. Interfaces*, 2016, **8**, 7471–7482.

9 Q. W. Jiang, G. R. Li, S. Liu and X. P. Gao, Surface-Nitrided Nickel with Bifunctional Structure as Low-Cost Counter Electrode for Dye-Sensitized Solar Cells, *J. Phys. Chem. C*, 2010, **114**, 13397–13401.

10 Z. Tachan, M. Shalom, I. Hod, S. Rühle, S. Tirosh and A. Zaban, PbS as a Highly Catalytic Counter Electrode for Polysulfide-Based Quantum Dot Solar Cells, *J. Phys. Chem. C*, 2011, **115**, 6162–6166.

11 J. Xu, X. Yang, Q.-D. Yang, T.-L. Wong and C.-S. Lee, Cu₂ZnSnS₄ Hierarchical Microspheres as an Effective Counter Electrode Material for Quantum Dot Sensitized Solar Cells, *J. Phys. Chem. C*, 2012, **116**, 19718–19723.

12 K. C. Sun, I. A. Sahito, J. W. Noh, S. Y. Yeo, J. N. Im, S. C. Yi, Y. S. Kim and S. H. Jeong, Highly Efficient and Durable Dye-Sensitized Solar Cells Based on a Wet-Laid Pet Membrane Electrolyte, *J. Mater. Chem. A*, 2016, **4**, 458–465.

13 I. A. Sahito, K. C. Sun, A. A. Arbab, M. B. Qadir and S. H. Jeong, Integrating High Electrical Conductivity and Photocatalytic Activity in Cotton Fabric by Cationizing for Enriched Coating of Negatively Charged Graphene Oxide, *Carbohydr. Polym.*, 2015, **130**, 299–306.

14 I. A. Sahito, K. C. Sun, A. A. Arbab, M. B. Qadir, Y. S. Choi and S. H. Jeong, Flexible and Conductive Cotton Fabric Counter Electrode Coated with Graphene Nanosheets for High Efficiency Dye-sensitized solar cell, *J. Power Sources*, 2016, **319**, 90–98.

15 B. Fang, S.-Q. Fan, J. H. Kim, M.-S. Kim, M. Kim, N. K. Chaudhari, J. Ko and J.-S. Yu, Incorporating Hierarchical Nanostructured Carbon Counter Electrode into Metal-Free Organic Dye-Sensitized Solar Cell., *Langmuir*, 2010, **26**, 11238–11243.

16 D.-Y. Kang, Y. Lee, C.-Y. Cho and J. H. Moon, Inverse Opal Carbons for Counter Electrode of Dye-Sensitized Solar Cells, *Langmuir*, 2012, **28**, 7033–7038.

17 S.-Q. Fan, B. Fang, J. H. Kim, B. Jeong, C. Kim, J.-S. Yu and J. Ko, Ordered Multimodal Porous Carbon as Highly Efficient Counter Electrodes in Dye-Sensitized and Quantum-Dot Solar Cells, *Langmuir*, 2010, **26**, 13644–13649.

18 A. A. Arbab, K. C. Sun, I. A. Sahito, A. A. Memon, Y. S. Choi and S. H. Jeong, Fabrication of Textile Fabric Counter Electrodes Using Activated Charcoal Doped Multi-walled Carbon Nanotube Hybrids for Dye-sensitized solar cells, *J. Mater. Chem. A*, 2016, **4**, 1495–1505.

19 Y. Liao, *et al.*, Facile Synthesis of High-Crystallinity Graphitic Carbon/Fe₃C Nanocomposites as Counter Electrodes for High-Efficiency Dye-Sensitized Solar Cells, *ACS Appl. Mater. Interfaces*, 2013, **5**, 3663–3670.

20 Z. A. Akbar, J.-S. Lee, H.-I. Joh, S. Lee and S.-Y. Jang, High-Efficiency FTO-Free Counter Electrodes for Dye-Sensitized Solar Cells Based on Low-Pt-Doped Carbon Nanosheets, *J. Phys. Chem. C*, 2015, **119**, 2314–2321.

21 B. Zhao, H. Huang, P. Jiang, H. Zhao, X. Huang, P. Shen, D. Wu, R. Fu and S. Tan, Flexible Counter Electrodes Based on Mesoporous Carbon Aerogel for High-Performance Dye-Sensitized Solar Cells, *J. Phys. Chem. C*, 2011, **115**, 22615–22621.

22 G. Veerappan, K. Bojan and S.-W. Rhee, Sub-Micrometer-Sized Graphite as a Conducting and Catalytic Counter Electrode for Dye-Sensitized Solar Cells, *ACS Appl. Mater. Interfaces*, 2011, **3**, 857–862.

23 Y.-Y. Li, C.-T. Li, M.-H. Yeh, K.-C. Huang, P.-W. Chen, R. Vittal and K.-C. Ho, Graphite with Different Structures as Catalysts for Counter Electrodes in Dye-Sensitized Solar Cells, *Electrochim. Acta*, 2015, **179**, 211–219.

24 S. Nagarajan, P. Sudhagar, V. Raman, W. Cho, K. Dhathathreyan and Y. S. Kang, A PEDOT-Reinforced Exfoliated Graphite Composite as a Pt-and TCO-Free Flexible Counter Electrode for Polymer Electrolyte Dye-Sensitized Solar Cells, *J. Mater. Chem. A*, 2013, **1**, 1048–1054.

25 Y. Li, H. Wang, Q. Feng, G. Zhou and Z.-S. Wang, Reduced Graphene Oxide–TaON Composite as a High-Performance Counter Electrode for Co(Bpy)₃^{3+/2+}-Mediated Dye-Sensitized Solar Cells, *ACS Appl. Mater. Interfaces*, 2013, **5**, 8217–8224.

26 L. Chen, C. X. Guo, Q. Zhang, Y. Lei, J. Xie, S. Ee, G. Guai, Q. Song and C. M. Li, Graphene Quantum-Dot-Doped Polypyrrole Counter Electrode for High-Performance Dye-Sensitized Solar Cells, *ACS Appl. Mater. Interfaces*, 2013, **5**, 2047–2052.

27 I. A. Sahito, K. C. Sun, A. A. Arbab, M. B. Qadir and S. H. Jeong, Graphene Coated Cotton Fabric as Textile Structured Counter Electrode for DSSC, *Electrochim. Acta*, 2015, **173**, 164–171.

28 J.-Z. Chen, C. Wang, C.-C. Hsu and I.-C. Cheng, Ultrafast Synthesis of Carbon-Nanotube Counter Electrodes for Dye-Sensitized Solar Cells Using an Atmospheric-Pressure Plasma Jet, *Carbon*, 2016, **98**, 34–40.

29 M. Zheng, J. Huo, Y. Tu, J. Wu, L. Hu and S. Dai, Flowerlike Molybdenum Sulfide/Multi-Walled Carbon Nanotube Hybrid as Pt-Free Counter Electrode Used in Dye-Sensitized Solar Cells, *Electrochim. Acta*, 2015, **173**, 252–259.

30 M.-H. Yeh, L.-Y. Lin, C.-L. Sun, Y.-A. Leu, J.-T. Tsai, C.-Y. Yeh, R. Vittal and K.-C. Ho, Multiwalled Carbon Nanotube@Reduced Graphene Oxide Nanoribbon as the Counter Electrode for Dye-Sensitized Solar Cells, *J. Phys. Chem. C*, 2014, **118**, 16626–16634.

31 W. Zhao, B. Tong, J. Shi, Y. Pan, J. Shen, J. Zhi, W. K. Chan and Y. Dong, Fabrication and Optoelectronic Properties of Novel Films Based on Functionalized Multiwalled Carbon Nanotubes and (Phthalocyaninato)Ruthenium(ɪɪ) *via* Coordination Bonded Layer-by-Layer Self-Assembly, *Langmuir*, 2010, **26**, 16084–16089.

32 W. J. Lee, E. Ramasamy, D. Y. Lee and J. S. Song, Efficient Dye-Sensitized Solar Cells with Catalytic Multiwall Carbon Nanotube Counter Electrodes, *ACS Appl. Mater. Interfaces*, 2009, **1**, 1145–1149.

33 B. Wang, S. Chang, L. T. L. Lee, S. Zheng, K. Y. Wong, Q. Li, X. Xiao and T. Chen, Improving Pore Filling of Gel Electrolyte and Charge Transport in Photoanode for High-Efficiency Quasi-Solid-State Dye-Sensitized Solar Cells, *ACS Appl. Mater. Interfaces*, 2013, **5**, 8289–8293.

34 W. Zheng, T. Qi, Y.-c. Zhang, H.-y. Shi and J.-q. Tian, Fabrication and Characterization of a Multi-Walled Carbon Nanotube-Based Counter Electrode for Dye-Sensitized Solar Cells, *New Carbon Mater.*, 2015, **30**, 391–396.

35 A. A. Arbab, K. C. Sun, I. A. Sahito, M. B. Qadir and S. H. Jeong, Multiwalled Carbon Nanotube Coated Polyester Fabric as Textile Based Flexible Counter Electrode for Dye-sensitized solar cell, *Phys. Chem. Chem. Phys.*, 2015, **17**, 12957–12969.

36 J. T. Han, *et al.*, Dispersant-Free Conducting Pastes for Flexible and Printed Nanocarbon Electrodes, *Nat. Commun.*, 2013, **4**, 2491.

37 A. A. Arbab, K. C. Sun, I. A. Sahito, M. B. Qadir and S. H. Jeong, Fabrication of Highly Electrocatalytic Active Layer of Multi-walled Carbon Nanotube/Enzyme for Pt-Free Dye-Sensitized Solar Cells, *Appl. Surf. Sci.*, 2015, **349**, 174–183.

38 S. Yusuf, M. Aziz, H. Hassan, T. Bandara, B.-E. Mellander, M. Careem and A. Arof, Phthaloylchitosan-Based Gel Polymer Electrolytes for Efficient Dye-Sensitized Solar Cells, *J. Chem.*, 2014, **2014**, 783023.

39 X. Wang, Y. Zhang, Q. Xu, J. Xu, B. Wu, M. Gong, J. Chu and S. Xiong, A Low-Cost Quasi-Solid DSSC Assembled with PVDF-Based Gel Electrolyte Plasticized by PC–EC & Electrodeposited Pt Counter Electrode, *J. Photochem. Photobiol., A*, 2015, **311**, 112–117.

40 M. Noor, M. Buraidah, S. Yusuf, M. Careem, S. Majid and A. Arof, Performance of Dye-Sensitized Solar Cells with (PVDF–HFP)–KI–EC–PC Electrolyte and Different Dye Materials, *Int. J. Photoenergy*, 2011, **2011**, 960487.

41 J.-K. Tsai, W. D. Hsu, T.-C. Wu, J.-S. Zhou, J.-L. Li, J.-H. Liao and T.-H. Meen, Dye-Sensitized Solar Cells with Optimal Gel Electrolyte Using the Taguchi Design Method, *Int. J. Photoenergy*, 2013, **2013**, 617126.

42 K. C. Sun, M. B. Qadir and S. H. Jeong, Hydrothermal Synthesis of TiO$_2$ Nanotubes and Their Application as an Over-Layer for Dye-Sensitized Solar Cells, *RSC Adv.*, 2014, **4**, 23223–23230.

43 M. B. Qadir, K. C. Sun, I. A. Sahito, A. A. Arbab, B. J. Choi, S. C. Yi and S. H. Jeong, Composite Multi-Functional Over Layer: A Novel Design to Improve the Photovoltaic Performance of DSSC, *Sol. Energy Mater. Sol. Cells*, 2015, **140**, 141–149.

44 J. Balamurugan, A. Pandurangan, R. Thangamuthu and S. M. Senthilkumar, Effective Synthesis of Well-Graphitized Carbon Nanotubes on Bimetallic SBA-15 Template for Use as Counter Electrode in Dye-Sensitized Solar Cells, *Ind. Eng. Chem. Res.*, 2013, **52**, 384–393.

45 P. Dong, *et al.*, Vertically Aligned Single-Walled Carbon Nanotubes as Low-Cost and High Electrocatalytic Counter Electrode for Dye-Sensitized Solar Cells, *ACS Appl. Mater. Interfaces*, 2011, **3**, 3157–3161.

46 J. D. Roy-Mayhew, D. J. Bozym, C. Punckt and I. A. Aksay, Functionalized Graphene as a Catalytic Counter Electrode in Dye-Sensitized Solar Cells, *ACS Nano*, 2010, **4**, 6203–6211.

47 X. Li, R. Chen, L. Li, S. Wang, W. Zhang, K. Wu, W. Li and M. Wu, A Comparative Evaluation of Catalytic Activities of Carbon Molecular Sieve Counter Electrode toward Different Redox Couples in Dye-Sensitized Solar Cells, *Electrochim. Acta*, 2016, **200**, 168–173.

48 G. Yue, J. Wu, Y. Xiao, M. Huang, J. Lin and J.-Y. Lin, High Performance Platinum-Free Counter Electrode of Molybdenum Sulfide–Carbon Used in Dye-Sensitized Solar Cells, *J. Mater. Chem. A*, 2013, **1**, 1495–1501.

49 S. Kuwahara, S. Taya, N. Osada, Q. Shen, T. Toyoda and K. Katayama, Effect of Electrolyte Constituents on the Motion of Ionic Species and Recombination Kinetics in Dye-Sensitized Solar Cells, *Phys. Chem. Chem. Phys.*, 2014, **16**, 5242–5249.

50 L. T. L. Lee, J. He, B. Wang, Y. Ma, K. Y. Wong, Q. Li, X. Xiao and T. Chen, Few-Layer MoSe$_2$ Possessing High Catalytic Activity Towards Iodide/Triiodide Redox Shuttles, *Sci. Rep.*, 2014, **4**, 4063.